DESIGN AND ANALYSIS OF THE MULTI-LEVEL INVERTERS WITH FAULT-TOLERANT CONTROL SYSTEM FOR THE POWER QUALITY IMPROVEMENT IN THE PV SYSTEM

Mr. R. Ranjith[1], G. Jayakrishna[2]

[1]*PG scholar in the Dept. of Electrical Electronics Engineering, Holy Mary Institute of Technology Science, Bogaram(V), Medchal District, Hyderabad, India.*

[2]*Professor in the Dept. of Electrical Electronics Engineering, Holy Mary Institute of Technology Science, Bogaram(V), Medchal District, Hyderabad, India.*

***Abstract*— In this paper, perturb and observe (P&O) based MPPT PV system with Multilevel inverter is analyzed with the fault tolerant control system. Since the application of MLI in a standalone photo-voltaic (PV) system requires constant DC voltages from PV panels, the MPPT strategy is deployed to regulate the voltage along with the capability to deliver the maximum power at full load. A multilevel converter is an electrical device that may offer several amounts of voltage levels at the output in order to make the output more comparable to a pure sine wave. The integrity of the multilevel converter depends on the reliability of individual switches such that the converter will collapse in case of faults in these switches. In this paper, a novel 9-level Fault-Tolerant Cascaded H-Bridge Multilevel Inverter (FT-CHB-MLI) has been proposed that offers high reliability with improved power quality. A dedicated Fault Detection and Isolation (FDI) unit has been built to diagnose the faulty switch and replace it with a standby redundant switch. Total Harmonic Distortion (THD) and the determination of a normalized output voltage factor are employed for fault diagnosis. The Phase Disposition Pulse Width Modulation (PD-PWM) technique has been utilized for switching due to its superior performance as compared to other conventional techniques.**

***Keywords*— perturb and observe (P&O), photo-voltaic (PV), Multilevel inverter, Fault-Tolerant Cascaded H-Bridge Multilevel Inverter (FT-CHB-MLI).**

1. INTRODUCTION

A. MULTILEVEL INVERTERS

Due to their appealing features, such as high-quality waveform and high nominal power, Multilevel Inverters (MLIs) have gained popularity among PV systems. As a result, several converters have been developed, including cascade H-bridge converters, neutral point clamped converters, and hybrid multilevel converters. These converters can be used in applications requiring medium and high power. Multilevel converters were originally used in the power train and high-voltage industrial applications. These converters were employed in utility-scale facilities for the first time in the renewable energy area, and they are still used on a wide scale in utility-scale plants today. If we split single-phase multilevel converters into three categories, we get Neutral Point Clamped (NPC), Continuous Feedback (CFB), and Cascaded H-Bridge (CHB) converters. When employed in a three-level converter, the diode-clamped converter is also known as the NPC since the mid-voltage level is specified as the neutral point level. The fundamental shortcoming of NPC converters in terms of the complete bridge is the requirement for dual dc-link voltage. An H-bridge is a pair of capacitors and switches that produces a different input DC voltage. MLIs are used for multiple purposes in voltage going from high level to medium level. Examples include their usage of magnetic levitation systems, electric traction, industrial applications, conveyors, and vacuum cleaners,

multiple gear systems, cooling systems, power plants, and smart houses. In multi-level inverters, stable voltage, fewer harmonics, noise, and better power factor having an improved power quality can be obtained by a small voltage step.

B. STRUCTURE OF A CASCADED H-BRIDGE MLI:

CHB MLI has a modular structure, which is one of the reasons why so many devices have this CHB MLI. By tinkering with the power cells, we may simply increase or reduce the power level of these inverters. The H-Bridge power cells are connected in series with one another, resulting in an increase in the inverter's power and voltage level. The structure of an MLI uses four devices for switching, each of which has a diode linked in reverse to it. A DC input voltage source is linked to each power cell. A Pulse Width Modulation (PWM) output waveform will be generated by these power cells. The waveform will be in the shape of stairs. The Cascaded H-bride inverter is divided into 2 types. They are:

1) Asymmetrical Cascaded H-Bridge MLI

2) Symmetrical Cascaded H-Bridge MLI

The input DC source is the basis for this division. An inverter is called a Symmetrical CHB inverter if it has equal valued DC voltage sources. In asymmetrical CHBMLI, unequal DC voltage sources are used. Examines a variety of devices and their reliability, as well as MLI mechanisms at all seven levels. A total of (n - 1) × 2 power devices used for switching and (n - 1)/2 multiple DC sources are needed for an n-level cascaded H-Bridge Multi-Level Inverter. The first cell's output voltage can be calculated as follows:

VCX1 = (S1 − S2) × Edc (1)

where Edc = DC voltage source VCX1 = Output voltage of the first power cell S1&S2 = Switches SW1 and SW2 for switching functions Additionally, add up to stage for M number of cells to calculate the desired output voltage associated with the arrangement.

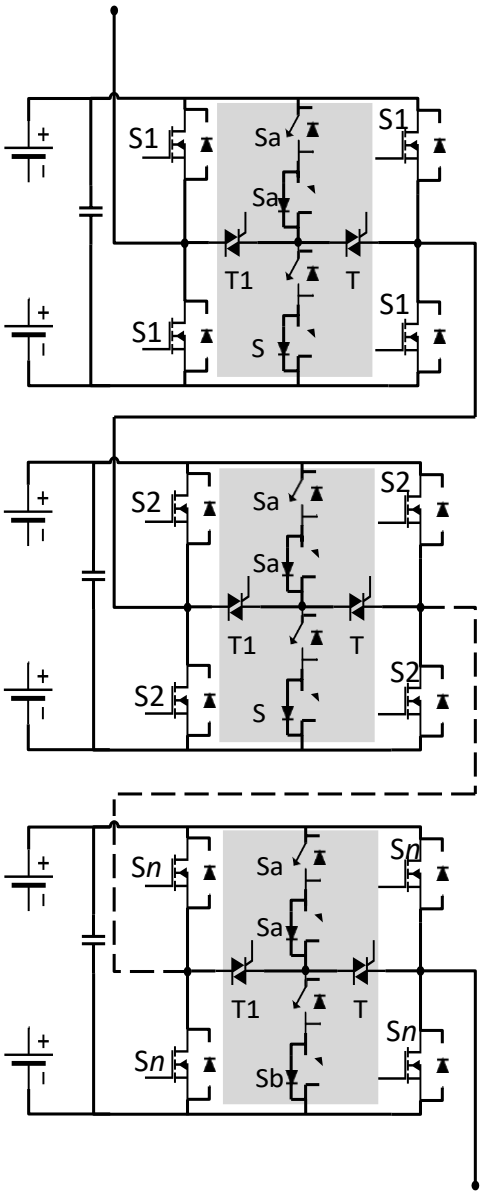

Fig 1. Schematic diagram of 9 levels cascaded H-Bridge multi-level inverter.

2. SYSTEM OVERVIEW

Photovoltaic system models have long time been an origin for the description of photovoltaic nature for researchers and professionals alike. The utmost ordinary model used to foresee energy generation in photovoltaic cell model is the single diode circuit [3, 15]. An ideal photovoltaic cell is comprised of a single diode connected in parallel with a light current source as depicted in Figure 1. A complete PV system simulation should fulfill the following criteria: (a) it should be simple and fast but able to correctively predict the *I-V* and *P-V* characteristic curves,

including special conditions such as partial shading; and (b) it should be an overall tool which can evolve and ratify a photovoltaic system design all-encompassing the power converter and the MPPT control as shown in Figure 2 [3].

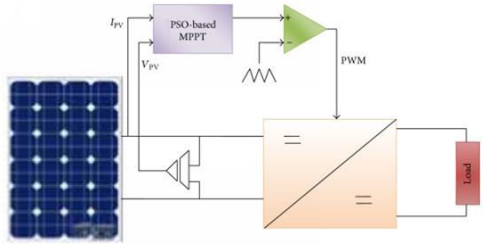

Figure 2 Configuration of the proposed PV system.

3. NOVEL CIRCUIT AND METHOD FOR FAULT RECONFIGURATION IN CASCADED H-BRIDGE MULTILEVEL INVERTER

A. Operating of the Proposed Circuit:

The proposed novel CHB topology presents a new approach to maintain system operation after multiple component failures. Figure 4.1 illustrates the summary of the presented approach. The idea is implemented by the highlighted relays and switches T1, T2, *Sa1, Sa2, Sb1*, and *Sb2*, etc. Once a fault has been detected using the method described in Chapter 3, these relays and switches enter the circuit operation to reconfigure the circuit in response to open/short circuit faults on *S11, S12, S13,* and *S14,* etc. This leads to an inverter that is capable of continued operation despite fault events. This is particularly significant when BESS is utilized for power delivery of safety critical infrastructure systems.

Oppositely, topologies proposed in the literature either have high implementation costs due to the use of a redundant battery or provide lower power quality with hardly noticeable enhancements to the reliability. The techniques of adding redundant cells would cause control difficulty for SOC balancing. Furthermore, prior fault-tolerant methods can only be applied to CHBs which are a sub-branch of MMCs. However, the presented approach can be applied to all types of MMCs.

The presented topology is implemented through an addition of four switches as displayed in Figure 4.1. T1 and T2 are either contactors or TRIACs, and are normally open. These switches and contactors are turned-on when the fault detection method indicates there is a fault. In case of a fault event in *Sn1* or *Sn3*, the switch *San* would begin operation to replace the faulty switch. Similarly, for faults in *Sn2* or *Sn4, Sbn* is turned-on in order to make up the lost switch. *San* and *Sbn* each consist of oppositely configured devices, and the reasons behind that is to avoid any current path through their anti-parallel diodes when the inverter operates under normal conditions. For better comprehension of this approach, assume the scenario when a fault has occurred in *S11* and the output voltage has lost one level. There are two main steps necessary for the presented topology to compensate the output voltage level. First, T1 or T2, depending on the fault location, needs to be turned on. Subsequently, the redundant switch respective to the faulty switch would begin operation using the same PWM signal as the failed switched. Hence the system would be capable of continuing seamless operation despite a fault.

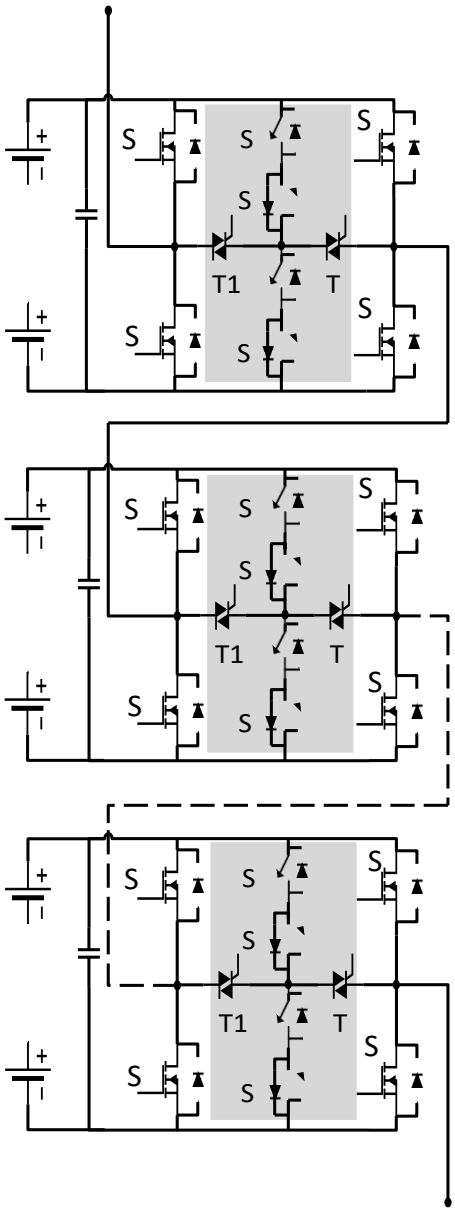

Fig 3. Schematic showing a novel reconfiguration CHB multilevel inverter.

B. Analysis of Fault-Tolerant Operation in Different Scenarios:

The proposed reconfiguration of the CHB inverter for fault-tolerant operation is shown in Figure 4.1. In normal operation, leg voltages could be expressed as a function of the upper or lowerswitches. The leg voltage from the 7-level cascaded H-Bridge inverter can be calculated as a function of the upper switches ($S_{n1}$and S_{n3}) as

$$V_{leg} = (S_{11} - S_{13})_1 + (S_{21} - S_{23})V_{dc2} + (S_{31} - S_{33})V_{dc3} \quad (4\text{-}1)$$

Also, from Table 3.1 in Chapter 3, the leg voltage could be expressed as a function of the lower switches (S_{n2} and S_{n4}) as

$$V_{leg} = (S_{14} - S_{12})_1 + (S_{24} - S_{22})V_{dc2} + (S_{34} - S_{32})V_{dc3} \quad (4\text{-}2)$$

To analyze the fault-tolerant operation of the CHB inverter, Figure 3 is examined with different fault scenarios. It is worth mentioning that the proposed topology is not limited to the following cases.

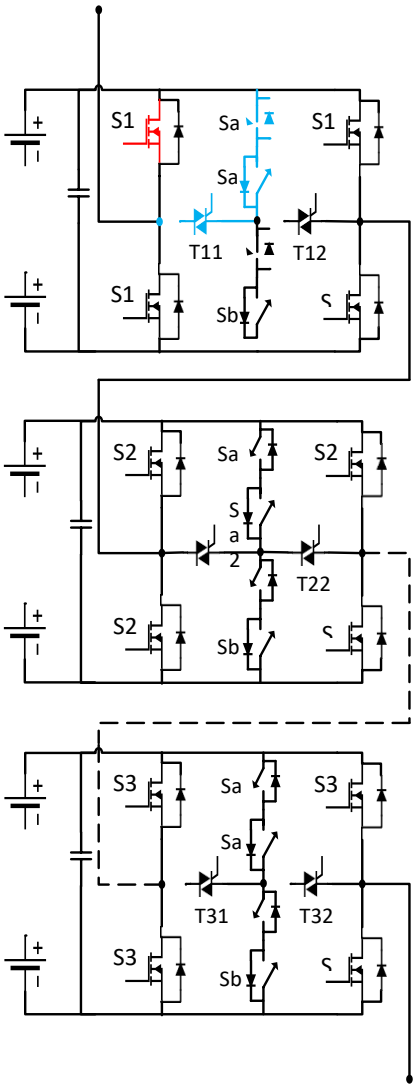

Fig 4 Reconfiguration and open-circuit faults switch on *S11*, where

blue lines indicatethe reconfigurable path and red lines indicate the fault location.

When $S11$ has an open-circuit fault and $i > 0$, the output voltage of the upper H-bridge of Figure is either $-V_{dc}$ or 0, and there are no possible positive voltages to be generated by the inverter.

That is, the anti-parallel diode of $S11$ is blocking the current path and restricting any positive outputvoltage.

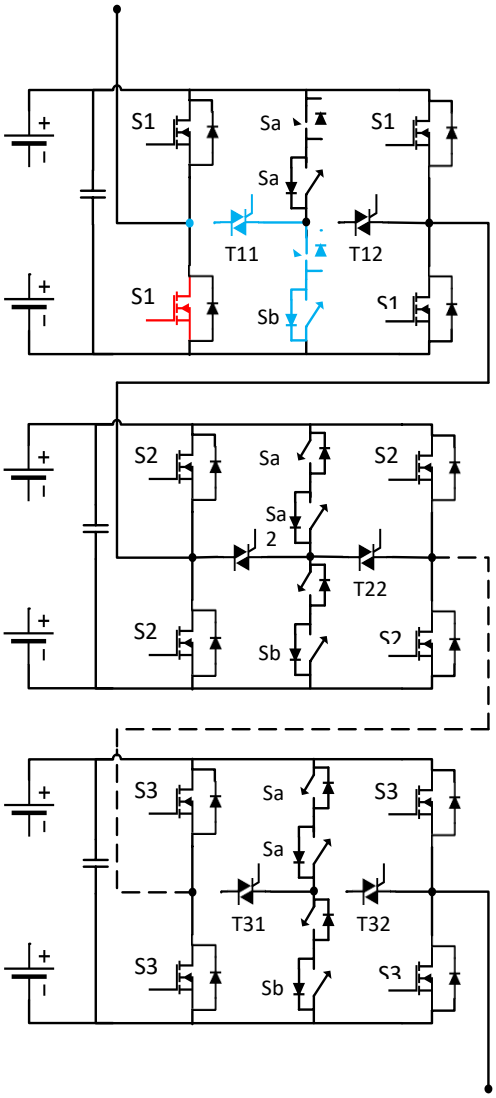

Fig 5. Reconfiguration and open-circuit faults switch on *S12*, where blue lines indicate the reconfigured path and red lines indicate the fault location.

Once the fault is detected, as described in Chapter 3, the reconfigurable circuit is activated through T1 and $Sa1$. That is, T1 is a normally open device, and when there is a fault on $S11$, T1 is turned on. The PWM for $Sa1$ is generated as the PWM signals for $S11$. Where the blue lines indicate the reconfigured path, and red lines indicate the fault location.

4. FAULT-TOLERANT CONTROL

Fault-Tolerant Control (FTC) techniques are used to increase machine dependability by avoiding occurrences that cause failure due to faults. A fault is defined as a variation in a system's output from its planned output, whereas a failure is defined as a full shutdown of a system. An FTC's primary function is to avoid malfunctions in important systems that might lead to their failure. Systems utilized for essential tasks such as unmanned aerial vehicles, planes, and nuclear power plants, cannot tolerate failure; hence, FTC is employed to increase the safety and dependability of such systems. One of the most significant components of the solar system's consistent functioning is the inverter's dependability. The advantages of a multi-level converter include reduced harmonic content in the output voltage, lower switching loss, and lower stress, making it the optimum choice for medium-high voltage and high power applications. However, because of the increased number of power switching devices, the multi-level inverter would raise the risk of a defect, lowering the system's dependability. Once the multi-level inverter fails, it will result in massive economic losses or catastrophic accidents. As a result, increasing the dependability of multilayer inverter systems is critical. One of the strategies used to construct an FTC system is redundancy, which is divided into two categories: analytical redundancy and hardware redundancy. Active and passive analytical redundancy are the two types of redundancy. The active analytical redundancy comprises fault detection, isolation, and controller reconfiguration, but it is complicated, computationally intensive, and sluggish

in performance; yet, it has the benefit of embracing a wide variety of defects. Because it is based on a strong controller design that can deal with the only considered uncertainties and faults in a system, passive analytical redundancy is a relatively simple and quick technique. However, it cannot handle a wide variety of defects.

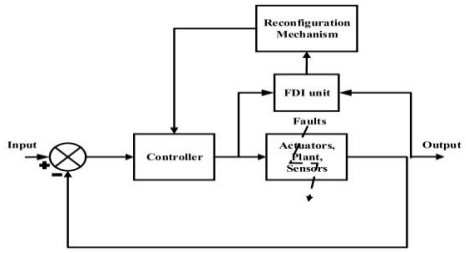

FIG 6. AFTCS Architecture [10].

The Fault Detection and Isolation (FDI) unit is the most important part of an Active Fault-Tolerant Control System (AFTCS), and it is responsible for detecting problems in actuators and sensors, as shown in Figure 2. The FDI unit is created by creating an observer model that creates estimated values that are utilized in the event of a component failure. The FDI performs controller reconfiguration after recognizing and isolating a malfunction by employing the estimated parameter values by the observer to adopt new circumstances. AFTCS has the benefit of supporting a wide range of defects and being an online fault detection-based system, but it is also complicated, computationally intensive, and slow to perfect.

The paper describes a defect detection transition control strategy based on a predictive model. An asymmetric zero voltage situation is required for an open-circuit problem diagnosis. The authors suggest a simpler approach that is based on zero-voltage switching and has been tested for both non-linear and linear loads. The authors offer a strategy for identifying short circuit defects based on an output voltage compared to the reference voltage of CHB MLIs with five levels (a neural network for a five-level CHB). A network based technique to defect detection is adopted. The authors in propose the use of MLIs to determine the kind of problem and its location, including five MLIs with several layers. The authors noted how, while MLIs have enticing properties, their large range of applications is constrained by the standard setup's usage of additional switches. With the fewest amount of unidirectional switches and gate trigger circuits, an elaboration on the contemporary 9-level MLI architecture is achieved, resulting in the lowest switching failures, as well as a smaller size and cheaper installation cost.

RELIABILITY ANALYSIS:

The suggested FT-CHB- MLI's reliability has been assessed using Markov chains in this section. The Mean Time to Failure is one of the most important quantitative indicators of a system's reliability. The mean time to failure (MTTF) of an item is displayed. It is the average amount of time that an item is predicted to last in service. The failed item has an indefinite repair time or simply cannot be fixed, according to the MTTF modelling assumption. The following formula is used to calculate MTTF

$$MTTF = \int_0^\infty R(t)\,dt$$

MTTF can also be calculated by taking the reciprocal of failure rate (λ) as follows

$$MTTF = \frac{1}{\lambda}$$

For the whole MLI assembly, we get

$\lambda 1 = (2N - 1)\,\lambda 0$

where λ0 is the failure rate of a single IGBT switch. By differentiation, we get

$dP1\ dt = -2\lambda 1 P1(t)$.

Hence, $R(t) = P1(t) = e^{-2(2N-1)\lambda 0 t}$

where N represents the number of switch modules in the MLI. Without fault tolerance, we get

$$MTTF_{without\ FTC} = \frac{1}{2\lambda_0}\left(\frac{1}{2N-1}\right)$$

$$\lambda_1 = \left(\frac{2N-1}{2}+1\right)\lambda_0$$

The failure rate of the two modules would be as follows:

$$\lambda_2 = \left(\frac{2N-1}{2}\right)\lambda_0$$

From Markov chains, we get

$$\frac{dP_1}{dt} = -\lambda_1 P_1(t)$$
$$P_1(t) = e^{-(\frac{2N-1}{2}+1)\lambda_0 t}$$
$$\frac{dP_1}{dt} = \lambda_1 P_1(t) - \lambda_2 P_2(t)$$
$$P_2(t) = \left(\frac{2N-1}{2}\right)\left(e^{-\left(\frac{2N-1}{2}\right)\lambda_0 t} - e^{-\left(\frac{2N-1}{2}+1\right)\lambda_0 t}\right)$$

The total reliability would be as follows:

$$R(t) = P_1(t) + P_2(t)$$
$$= \left(\left(\frac{1-2N}{2}\right)e^{-\left(\frac{2N-1}{2}+1\right)\lambda_0 t}\right) + \left(\frac{2N-1}{2}\right)\left(e^{-\left(\frac{2N-1}{2}\right)\lambda_0 t}\right)$$

$$MTTF_{withFTC1} = \frac{1}{\lambda_0}\left(\frac{1-N}{N+1}\right)$$
$$\lambda_2 = (2N-3)\lambda_0$$
$$\frac{dP_1}{dt} = -(\lambda_1+\lambda_2)P_2(t) - \lambda_1 P_1(t)$$
$$P_2(t) = \left(\frac{2N-3}{2}\right)\left(e^{-(\lambda_1+\lambda_2)t} - e^{-2\lambda_1 t}\right)$$
$$\frac{dP_4}{dt} = -(2\lambda_2)P_4(t) + \lambda_1 P_2(t) + \lambda_1 P_3(t)$$
$$P_4(t) = \frac{(2N-3)^2}{4}\left(e^{-2\lambda_1 t} + e^{-2\lambda_2 t}\right) - \frac{(2N-3)^2}{2}e^{-(\lambda_1+\lambda_2)t}$$
$$R(t) = P_1(t) + P_2(t) + P_3(t) + P_4(t)$$
$$R(t) = \left((2N-2) + \frac{(N-3)^2}{4}\right)e^{-2(2N-1)\lambda_0 t} + \left((2N-3) + \frac{(2N-3)^2}{4}\right)e^{-2(2N-2)\lambda_0 t} + \left(\frac{(2N-3)^2}{4}\right)e^{-2(2N-3)\lambda_0 t}$$
$$MTTF_{with\ FTC} = \frac{1}{2\lambda_0}\left(\frac{\left((2N-2)+\frac{(2N-3)^2}{4}\right)}{(2N-1)} + \frac{\left((2N-3)+\frac{(2N-3)^2}{4}\right)}{(2N-2)} + \frac{\left(\frac{(2N-3)^2}{4}\right)}{(2N-3)}\right)$$

The equation demonstrates that the MTTF has significantly increased with the proposed FT-CHB-MLI architecture.

5. Particle Swarm Optimization PSO

Particle swarm optimization (PSO) is a stochastic, population-based EA search method, modeled after the behavior of bird flocks [13]. The PSO algorithm maintains a swarm of individuals (called particles), where each particle represents a candidate solution. Particles follow a simple behavior: emulate the success of neighboring particles and its own achieved successes. The position of a particle is therefore influenced by the best particle in a neighborhood, p_{best}, as well as the best solution found by all the particles in the entire population, g_{best}. The particle position x_i, is adjusted using [13]

$$x_i^{t+1} = x_i^t + v_i^{t+1}$$

where the velocity component, vi , represents the step size.

The velocity is calculated by

$$v_i^{t+1} = wv_i^t + c_1 r_1 \cdot \left(p_{\text{best}}, i - x_i^t\right) + c_2 r_2 \cdot \left(g_{\text{best}} - x_i^t\right), \quad i = 1, 2, \ldots, N,$$

where xi denote the particle position for i ; the velocity of the particle at i is represented by vi, the number of iteration is denoted by t; the inertia weight is represented by w:r1 and r2 are uniformly distributed random variables within[0,1] ; and the cognitive and social coefficient are, respectively, denoted by (c1c2) [14]. The best position for the storage of the th particle that has been found so far is denoted by variable pbesti and the storage of the best position of all the particles is represented by gbest . Figure 3 depicts the movement of particle in the optimization process.

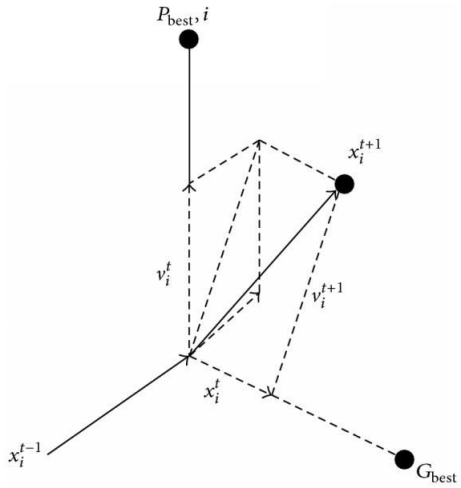

Fig7. The Weakness of Conventional Particle Swarm Optimization-Based MPPT Techniques

Conventional PSO is fast and accurate when searching for the output characteristic curves of PV module

arrays with single peak values. However, when some modules are shaded, weights in conventional PSO must be readjusted appropriately based on various multipeak curve characteristics. If this is not performed, excessively high or low weights result in tracking failure. Thus, conventional PSO-based MPPT must be modified when some of the modules in a photovoltaic module array are shaded.

6. PSO-BASED MPPT TECHNIQUE

For the IPSO-based MPPT system designed, the position of the particle is designated as the duty cycle of the power converter, while the fitness value evaluation function was chosen as the produced power Ppv for the entire photovoltaic system. In the proposed method overview, more accurate MPP tracking is achieved despite the complex shading conditions with the smaller particle number and where larger number of particles results in lengthy computation time. Therefore, for good tracking speed and accuracy to be ensured, a trade off should be made. According to some research, at most there exist m MPPs in the *P-V* curve for photovoltaic modules which consist of m series connected photovoltaic cells [12]. For initialization step of the particle swarm optimization, particles could be established in the random range or be placed on stationary position. Mostly, it makes more sense to initialize the particles around it if there is data available regarding the position of the global maximum power point in the search range. In [12], the authors state that the minimum displacement between successive peaks is nearly 80% of Voc and also the peaks on the *P-V* curve occur nearly at multiples of 80% of the module open voltage Voc. Thus, the number of particle N is selected in the photovoltaic system as the number of the series connected cells. The search spaces of the particles that cover [0 1] are initialized on definite point. 0 and 1 are the duty cycle minimum and maximum value of the dc-dc converter used, respectively.

The objective of this IPSO-based MPPT method was to extract the maximum power Ppv of the photovoltaic. To evaluate the fitness value which is the generated power, after the controller output, the pulse width modulation acts in line to the particle position I that denote the duty cycle state, and the photovoltaic voltage Vpv and current Ipv can be measured. To calculate the fitness value Ppv of particle i , these values can then be used. However, to obtain the right samples time, it should be noted that power converter's settling time has to be lesser than the evaluations time interspaces between subsequent particles.

To address these problems, linear decreases with increasing iteration numbers were adopted in this study for the weighting of the PSO formulas. The physical meaning of this modified weighting formula is that greater step sizes are used to increase the particle search velocity during the initial search because the distance to the global optimum is relatively large. This prevents an excessively small step size from making local optimum traps unavoidable. However, w decreases gradually as the number of iterations increases. Because the particles are now approaching the MPP, these decreases in w cause the steps in the particle movements to shrink, enabling the particles to track the MPP more accurately.

In (5), in order to maintain the particle accelerating in the same direction it was originally moving, the first term w(t) vi(t) is therefore utilized, where the converging demeanor of the particle swarm optimization is controlled. The inertia weight will be chosen in order to accelerate convergence, such that the effect of vi(t) diminished through the process of the algorithm. Hence, the choice of a decreasing value of w with time is considered. To get refined solutions, a typical option is to set the inertia weight initially to a bigger value and slowly reduce it for better exploration. For this reason, here, the term w was used as linearly decreasing scheme, as illustrated as follows:

$$w(t) = w_{\max} - \frac{t}{t_{\max}}(w_{\max} - w_{\min})$$

In (6), the minimum and maximum bounds of w were denoted by wmin and wmax, while the maximum allowed number of iterations are denoted by tmax. Likewise, the social and cognitive terms can be remodelled. In (5), the search ability of particle swarm optimization can be affected by the values of c1 and c2 by changing the particle direction. Selecting c1>c2 sampling with respect to the bearing of pbesti would be biased, while selecting c1<c2 in the reverse case, sampling in respect to the bearing of gbesti will be preferred. For these reasons, these two terms are defined as continuously increasing and continuously decreasing functions, as in (7) and (8) respectively:

$$c_1(t) = c_{1,\max} - \frac{t}{t_{\max}}\left(c_{1,\max} - c_{1,\min}\right),$$

$$c_2(t) = c_{2,\max} - \frac{t}{t_{\max}}\left(c_{2,\max} - c_{2,\min}\right).$$

Two convergence criteria are employed in this study. The proposed IPSO-based MPPT method will halt and yield the gbest solution, if the maximum number of iterations is attained or if all the particles velocities become smaller than a threshold.

Basically, particle swarm optimization algorithms are utilized to address optimization difficulty that the optimum result is time invariant. However, in this case, the fitness value which is the global maximum power point sometimes varies or depends on environmental factors as well as loading states. To search for the new global MPP again in these cases, the particles must be reinitialized. Considering the change in insolation and shading pattern to be detected, here, the following constraint is utilized. In the proposed IPSO-based technique, the particles will be reinitializing whenever the following condition is satisfied as shown in (9); Figure 4 depicts the comprehensive flowchart of the proposed system:

$$\frac{\left|P_{\text{PV, new}} - P_{\text{PV, old}}\right|}{P_{\text{PV, old}}} \geq \Delta P\,(\%)\,,$$

where Ppvnew is the new photovoltaic power, Ppvold is the photovoltaic power at global maximum point of the last operating point, and $\Delta P\%$ is set to 10%.

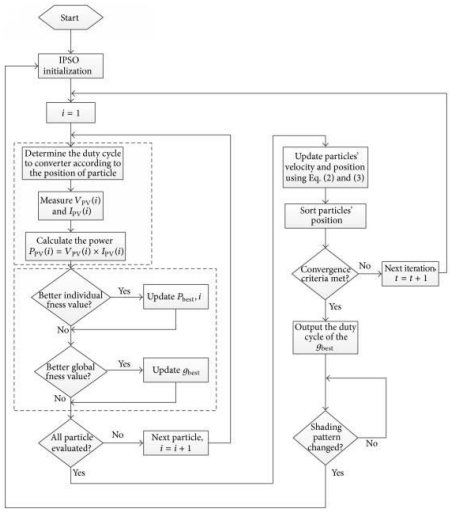

Figure 8. Flowchart of the proposed PSO-based MPPT algorithm.

7. SIMULATION RESULTS

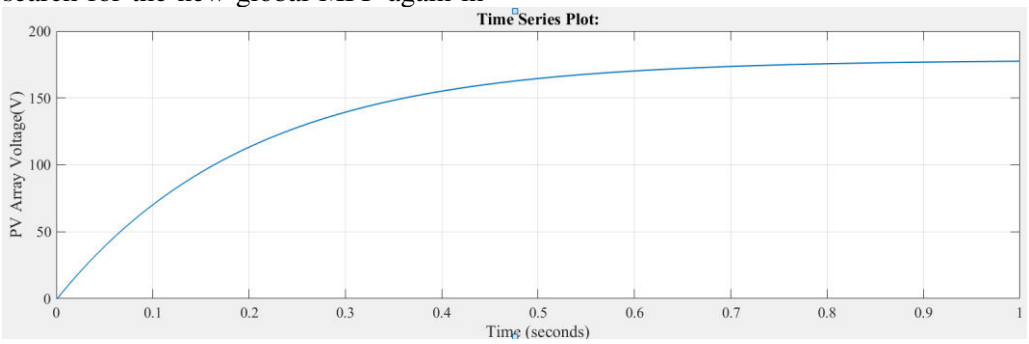

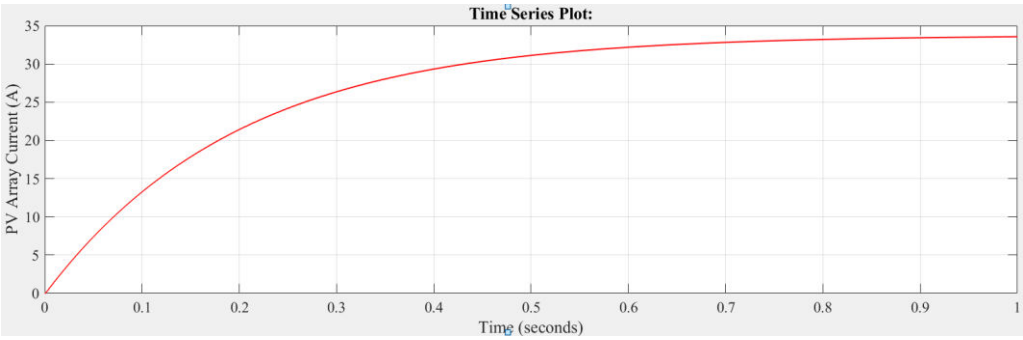

Fig9. Solar PV Array Voltage and current Output wave forms.

In the Fig the PV array Voltage and the Current of each panel is shown with the Voltage of 180V and currents of 35A of each panel.

The simulation results of the output power of the PV panel using the P&O process controller at steady temperature (T = 25 °C) and irradiance (E = 1,000 w/m2) indicate that the P&O solution provides 94% performance. As the irradiation switches quickly, however, the P&O controller has a better time response process.

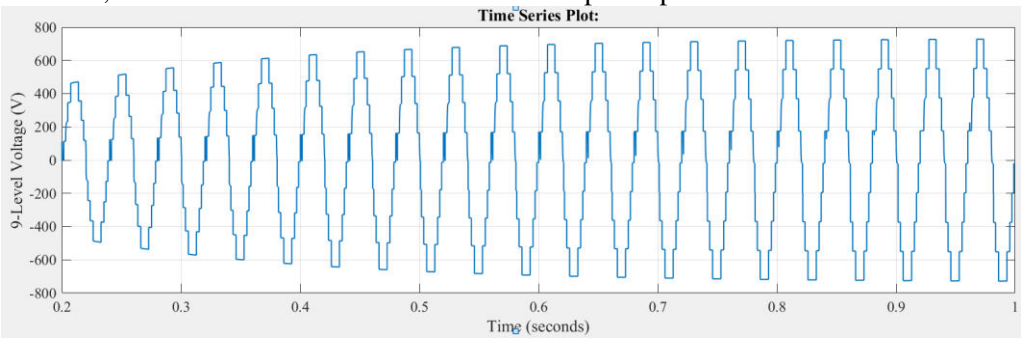

Fig10. 9 level Inverter Voltage is 720V

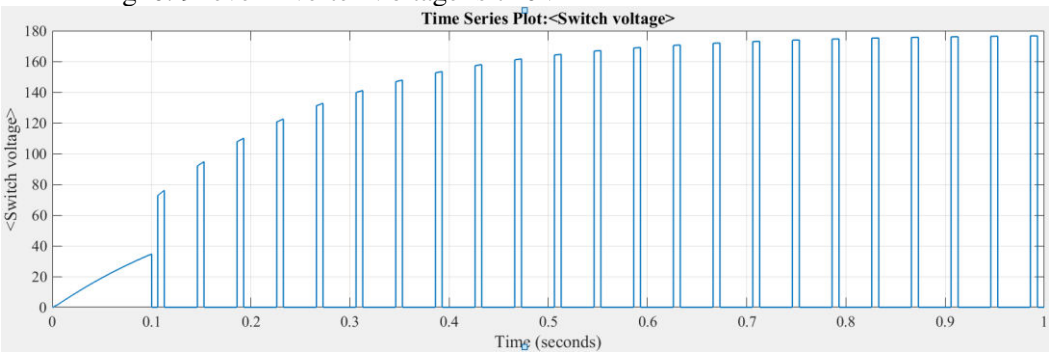

Fig10. Switching Voltage without Fault case

The results show that the output is affected at 0.1 seconds at the time of fault injection but returns to its normal operation due to the switch over of the faulty switch to the healthy standby IGBT switch.

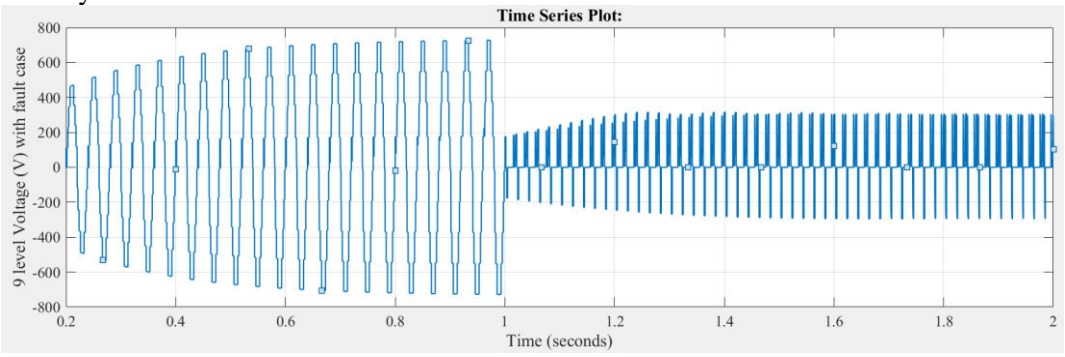

Fig11. 9 level Inverter Voltage with Fault case

The switching states of both primary and standby IGBTs after the occurrence of fault are shown in Figure 20 which shows the operation of the redundant switch due to the failure of the primary switch.

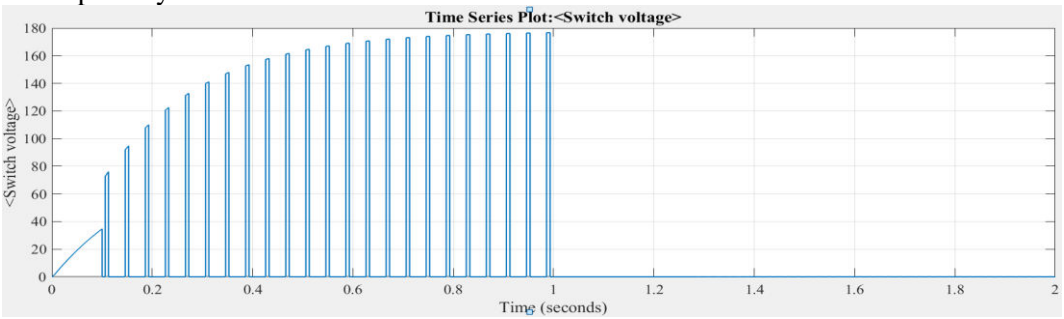

Fig12. 9 level Inverter Switching Voltage with Fault case

Voltage with Fault case

The output voltages of the proposed 7-level cascaded MLI are shown in Figure 14. These output voltages have a magnitude of 300V (peak). As in this situation, there is no fault applied at any switch of the MLI, therefor output voltages are equal throughout the simulations. The switching signals to the primary IGBTs during normal operation are shown in Figure 15. The standby redundant IGBTs remain in the off condition with no switching signal. The THD has been measured using the FFT tool of Simulink. Figure 16 shows a total THD of 18.53% for the normal operation of this CHD MLI. Now the fault is injected by the FIU at 0.1 seconds and the resulting output waveform is shown in Figure 17. The positive peak voltage has reduced to around 200 V and total THD has also increased to 19.2% as shown in Figure 18. Now the system has been simulated with FTC CHB MLI configuration and the resulting waveform. The results show that the output is affected at 0.1 seconds at the time of fault injection but returns to its normal operation due to the switch over of the faulty switch to the healthy standby IGBT switch. The switching states of both primary and standby IGBTs after the occurrence of fault are shown in Figure 20 which shows the operation of the redundant switch due to the failure of the primary switch. The THD of the output waveform of FT CHB MLI is shown in Figure 21 which shows the improvement from 19.2% to 18.55% by the proposed control system. Hence, the objective of reliability enhancement with improved power quality has been successfully achieved.

8. COMPARISON WITH EXISTING WORKS:

In this section, a comparison of the proposed FT-CHM-MLI has been performed to demonstrate its superior performance. In [16], a fault-tolerant H-bridge system is proposed for DC motor speed control with the PWM technique only resulting in a very large harmonics content of about 48.3% in the output waveform which makes the proposed solution not feasible from the power quality point of review through its highly reliable. The solution proposed in [29], FT-CHB is proposed but it is only for five levels that also results in a high THD of 20.83% which is not up to the mark. In this proposed work, the THD has been reduced to almost 18% with a significant increase in reliability with advanced fault-tolerant architecture consisting of an FDI unit.

CONCLUSION

In this paper, a novel 9-level Fault-Tolerant Cascaded H-Bridge Multilevel Inverter (FT-CHB-MLI) with the PV array system with the PSO MPPT method was proposed that offers high reliability with improved power quality. A dedicated Fault Detection and isolation (FDI) unit was built to diagnose the faulty switch and replace it with a standby redundant switch. Total harmonic distortion and the determination of a normalized output voltage factor were employed for fault diagnosis. The Phase Disposition Pulse Width Modulation (PD-PWM)

technique was utilized for switching due to its superior performance as compared to other conventional techniques. The proposed system was experimentally tested on the MATLAB / Simulink environment to verify its performance. The simulation results demonstrated that the THD has been reduced to almost 18% with a significant increase in reliability with advanced fault-tolerant architecture consisting of FDI units. The reliability analysis was carried out using Markov chains that also showed its increased reliability.

REFERENCES

[1] A. Sinha, M. Shahbaz, and T. Sengupta, "Renewable energy policies and contradictions in causality: a case of next 11 countries," Journal of Cleaner Production, vol. 197, pp. 73-84, Oct. 2018.

[2] J. Macaulay, Z. Zhou, J. Macaulay et al., "A fuzzy logical-based variable step size P&O MPPT algorithm for photovoltaic system," Energies, vol. 11, no. 6, p. 1340, May 2018.

[3] N. Kumar, I. Hussain, B. Singh et al., "Single sensor-based MPPT of partially shaded PV system for battery charging by using cauchy and gaussian sine cosine optimization," IEEE Transactions on Energy Conversion, vol. 32, no. 3, pp. 983-992, Sept. 2017.

[4] E. E. A. Zahab, A. M. Zaki, and M. M. El-Sotouhy, "Design and con- trol of a standalone PV water pumping system," Journal of Electrical Systems and Information Technology, vol. 4, no. 2, pp. 322-337, Sept. 2017.

[5] G. Panayiotou, S. Kalogirou, and S. Tassou, "Design and simulation of a PV and a PV-wind standalone energy system to power a house- hold application," Renewable Energy, vol. 37, no. 1, pp. 355-363, Jan. 2012.

[6] P. M. Armstrong, R. Wong, R. Kang et al., "A reconfigurable PV array scheme integrated into an electric vehicle," in Proceedings of IET Hybrid and Electric Vehicles Conference 2013, London, UK, Nov. 2013, pp. 1-7.

[7] A. R. Abbaspour, ''Active fault-tolerant control design for nonlinear systems,'' M.S. thesis, FIU Electron., 2018, vol. 3917. [Online]. Available: https://digitalcommons.fiu.edu/etd/3917

[8] Z. Ji, J. Zhao, Y. Sun, X. Yao, and Z. Zhu, ''Fault-tolerant control of cascaded H-bridge converters using double zero-sequence voltage injection and DC voltage optimization,'' J. Power Electron., vol. 14, no. 5, pp. 946–956, Sep. 2014.

[9] A. A. Amin and K. M. Hasan, ''A review of fault tolerant control systems: Advancements and applications,'' Meas., J. Int. Meas. Confederation, vol. 143, pp. 58–68, Sep. 2019, doi: 10.1016/j.measurement.2019. 04.083.

[10] R. F. Stengel, ''Intelligent failure-tolerant control,'' IEEE Control Syst. Mag., vol. 11, no. 4, pp. 14–23, Jun. 1991.

AUTHOR DETAILS

Mr. R. Ranjith received the B. Tech Degree in Electrical And Electronics Engineering from Mahaveer Institute Of Science and Technology Keshavagiri (V), Bandlaguda (M), Hyderabad (Dist), Telangana, India. And Studying M. tech in Power Electronics at Holy Mary Institute of Technology and Science, Bogaram(V), Medchal (D), Hyderabad, India in the Dept. of Electrical & Electronics Engineering.

G. Jayakrishna has received his B. Tech degree in Electrical and Electronics Engineering and M. Tech in Electrical Power Systems from JNTU, Hyderabad and Ph.D. Degree in Electrical Engineering from JNTUA, Anantapur, Andhra Pradesh, India. Presently he is working as Professor in the Department of Electrical and Electronics Engineering, Holy Mary Institute of Technology and Science, Hyderabad, Telangana. He is having 25 years of teaching experience. His research interests include Power quality improvement, AI Techniques and renewable energy sources.